AIP | Applied Physics Letters

Tunable ultracompact chip-integrated multichannel filter based on plasmon-induced transparencies

Xiaoyu Yang, Xiaoyong Hu, Zhen Chai, Cuicui Lu, Hong Yang, and Qihuang Gong

Citation: Applied Physics Letters **104**, 221114 (2014); doi: 10.1063/1.4882916
View online: http://dx.doi.org/10.1063/1.4882916
View Table of Contents: http://scitation.aip.org/content/aip/journal/apl/104/22?ver=pdfcov
Published by the AIP Publishing

Tunable ultracompact chip-integrated multichannel filter based on plasmon-induced transparencies

Xiaoyu Yang,[1] Xiaoyong Hu,[1,2,a)] Zhen Chai,[1] Cuicui Lu,[1] Hong Yang,[1] and Qihuang Gong[1,2,a)]
[1]*State Key Laboratory for Mesoscopic Physics and Department of Physics, Peking University, Beijing 100871, People's Republic of China*
[2]*Collaborative Innovation Center of Quantum Matter, Beijing 100871, People's Republic of China*

(Received 14 April 2014; accepted 30 May 2014; published online 6 June 2014)

Nanoscale multichannel filter is realized in plasmonic circuits directly, which consists of four plasmonic nanocavities coupled via a plasmonic waveguide etched in a gold film. The feature device size is only 1.35 μm, which is reduced by five orders of magnitude compared with previous reports. The optical channels are formed by transparency windows of plasmon-induced transparencies. A shift of 45 nm in the central wavelengths of optical channels is obtained when the plasmonic coupled-nanocavities are covered with a 100-nm-thick poly(methyl methacrylate) layer. This work opens up the possibility for the realization of solid quantum chips based on plasmonic circuits. © *2014 AIP Publishing LLC*. [http://dx.doi.org/10.1063/1.4882916]

Recently, plasmon-induced transparency (PIT), a strong destructive interference coupling between wide-band superradiant states and narrow-band subradiant states in plasmonic nanostructures,[1] has attracted enormous attention because of its important applications in nanophotonics, quantum optics, and integrated photonic devices. A sharp narrow transmission window within a relatively broadband stop band is the signature of this phenomenon.[2] Various schemes have been presented to realize PIT in plasmonic nanostructures, such as using gold nanowire gratings,[3,4] metamaterials,[5–9] plasmonic slot antennas,[1,10] and plasmonic nanoresonators.[11] However, the PIT effect was reached in the direction perpendicular to the chip surface.[1–11] Moreover, periodic arrays of plasmonic nanostructures are used to obtain remarkable PIT effect.[1–11] This has seriously restricted the practical on-chip integration applications of PIT. To meet the requirements of integrated photonic chips, the PIT effect had to be realized in the direction parallel to the chip surface.[12] Though the phase coupling mechanism and near-field coupling mechanism have been proposed to demonstrate on-chip PIT, small experiment progress has been achieved up to now.[13–18] Part of the reason lies in that it is difficult to obtain remarkable on-chip PIT effect only using several plasmonic nanostructures.[17] Recently, Han *et al*. reported a on-chip PIT in a plasmonic waveguide side-coupled two plasmonic racetrack microcavities with a diameter of 4 μm etched in a gold film coated with a 300-nm-thick organic polymer layer.[19] To date, it is still a great challenge to realize integrated photonic devices based on on-chip PIT.

Here, we study how to realize a tunable ultracompact multichannel filter based on on-chip PIT in plasmonic circuits directly. For this purpose, we adopted four different plasmonic nanocavities coupled via a plasmonic waveguide etched in a gold film, as shown in Fig. 1(a). The on-chip PIT was realized by using the phase coupling mechanism. There is a phase accumulation ϕ for guided surface plasmon polaritons (SPPs) propagating between two near-neighboring nanocavities, which can be calculated by the relation[13]

$$\phi = \omega n_{\text{eff}} s/c, \tag{1}$$

where ω is the frequency of the guided SPPs, s is the distance between the two plasmonic nanocavities, and c is the light velocity in vacuum. Based on the coupled-mode theory, the transmitted power amplitude P_t of the guided SPP mode can be calculated by the relation[13]

$$P_t = -e^{i\phi}(-P_i - i\kappa a_1) - i\kappa a_2, \tag{2}$$

where P_i is the input power amplitude of the guided SPPs, κ is the fraction of power coupling into the plasmonic waveguide, and a_1 and a_2 are time-harmonic energy amplitudes of the two plasmonic nanocavities, respectively. It is very clear that a high transmission peak can be obtained in the transmission stop band for a proper phase accumulation ϕ, which leads to the generation of on-chip PIT effect.[13] The transparency window forms perfect optical channel of the filter. Multiple optical channels could be obtained when four different plasmonic nanocavities were introduced in series. A shift of 45 nm in the central wavelengths of optical channels was obtained when the plasmonic coupled-nanocavities were covered with a 100-nm-thick poly(methyl methacrylate) (PMMA) layer. Moreover, the central wavelengths of optical channels can also be tuned by adjusting the ambient temperature based on the thermo-optic effect of PMMA.

The three-dimensional schematic structure of the plasmonic coupled-nanocavities is shown in Fig. 1(b). The plasmonic waveguide was constructed from an air nanogroove with a width of 100 nm and a depth of 150 nm etched in a 300-nm-thick gold film deposited on silicon dioxide substrate. Four plasmonic nanocavities were constructed from air nanogrooves having a configuration of rectangular stub with a width of 100 nm and a depth of 150 nm etched in the 300-nm-thick gold film, as shown in Figs. 1(a) and 1(b). The

[a)]Authors to whom correspondence should be addressed. Electronic addresses: xiaoyonghu@pku.edu.cn and qhgong@pku.edu.cn

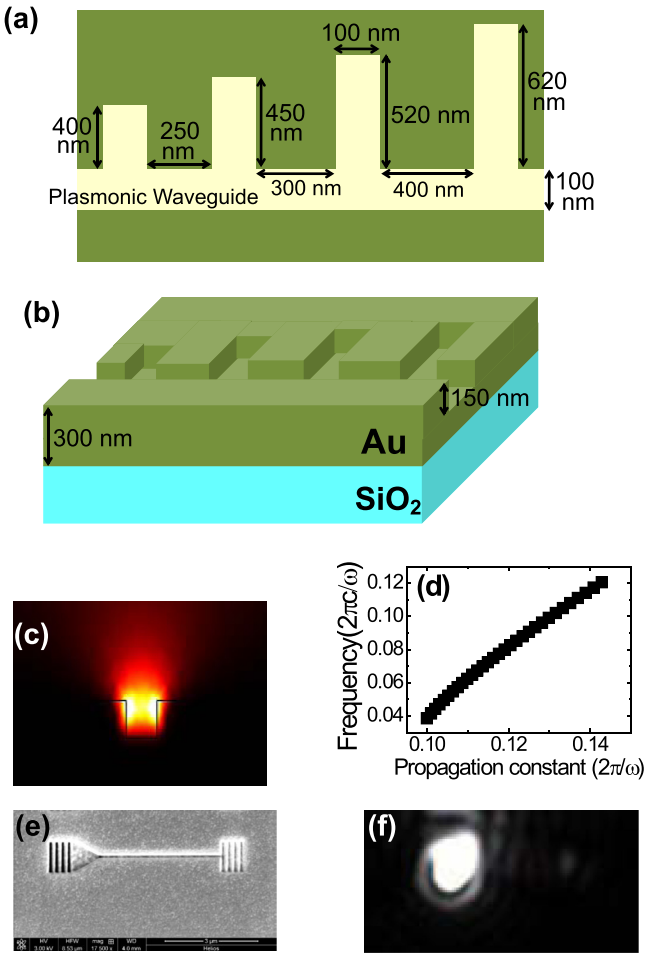

FIG. 1. Characterization of the plasmonic coupled-nanocavities without the PMMA cover layer. (a) Top-view schematic structure of the plasmonic coupled-nanocavities. (b) Three-dimensional schematic structure of the plasmonic coupled-nanocavities. (c) Calculated power density profile of the SPP mode excited by an 800 nm incident light. (d) Dispersion relations of the plasmonic waveguide. (e) SEM image of a 5-μm-long plasmonic waveguide. (f) Measured CCD image of the 5-μm-long plasmonic waveguide under excitation with an 800 nm CW laser beam.

length was 400, 450, 520, and 620 nm for four nanocavities, respectively. The interval between two near-neighboring nanocavities was 250, 300, and 400 nm, respectively, as shown in Fig. 1(a). To confirm the propagation properties of guided SPP modes in the plasmonic waveguide, we calculated the power density profile (Fig. 1(c)) of the SPP mode excited by a continuous-wave (CW) incident light with a wavelength of 800 nm by using the finite element method (adopting a commercial software package COMSOL Multiphysics).[20] The guided SPP mode was mainly confined in the nanogroove region, while extending into the upper air region. The maximum intensity was situated in the interface of gold and air around two upper corners of the nanogroove, which is in agreement with the calculations of Li *et al.*[21] To confirm the waveguiding properties of the plasmonic waveguide, we also calculated the dispersion relations (Fig. 1(d)) of the plasmonic waveguide by using the finite element method. The refractive index of air was set to be 1, while the frequency-dependent complex refractive index of gold was obtained from Ref. 22. The plasmonic waveguide could provide wideband guided SPP modes, as confirmed by the calculations of Li *et al.*[21]

The gold films with a thickness of 300 nm were fabricated by using a laser molecular beam epitaxy growth system (Model LMBE 450, SKY Company, China). The beam (with wavelength of 248 nm, pulse width of 25 ns, and pulse repetition rate of 5 Hz) output from an excimer laser system (Model COMPexPro 205, Coherent Company, USA) was focused on a gold target mounted on a rotating holder, situated 17 mm away from the silicon dioxide substrates. The typical energy density of the excitation laser was 430 mJ/cm^2. A focused ion beam etching system (Model Helios NanoLab 600, FEI Company, USA) was used to prepare the plasmonic waveguide and nanocavities. To further confirm the propagation properties of the guided SPP modes, we etched a 5-μm-long plasmonic waveguide in a 300-nm-thick gold film deposited on silicon dioxide substrate, as shown in Fig. 1(e). To efficiently excite and collect the required SPP mode, we also etched a coupling grating with a lattice constant of 500 nm connected to a triangular air groove in the input port of the plasmonic waveguide. For the coupling grating, the length, width, and depth of the air nanogrooves were 1 μm, 250 nm, and 300 nm, respectively. The depth of the triangular air groove was 150 nm. We also etched a decoupling grating with a depth of 150 nm in the output port of the plasmonic waveguide to help scatter the guided SPP modes into free space for the purpose of measurement. In our experiment, we adopted a nano-spectroscopy measurement system to measure the transmission properties of the plasmonic waveguide.[23] A p-polarized CW Ti:sapphire laser system (Model Mira 900F, Coherent Company, USA) was used as the light source. The line width of the laser spectrum of an 800 nm incident CW laser was only 1.6 nm, which guarantees that only the needed quasi-monochromatic SPP mode can be excited in the plasmonic waveguide. The coupling grating was normally illuminated from the back side. The optically thick gold film could prohibit direct transmission of the incident light. The SPP mode propagating through the plasmonic waveguide was scattered by the decoupling grating. The scattered light was collected by using a long working distance objective (Mitutoyo 20, NA = 0.58) and then detected by a charge coupled device (CCD). Figure 1(f) shows the measured CCD image of the 5-μm-long plasmonic waveguide under excitation with an 800 nm CW laser. Strong scattered light was obtained from the decoupling grating, which confirms the perfect propagation properties of the guided SPP modes.

To study the linear transmission properties of the plasmonic coupled-nanocavities, we measured the linear transmission spectrum of the plasmonic waveguide side-coupled four plasmonic nanocavities (depicted in Fig. 2(a)) by using the nano-spectroscopy measurement system, and the measured results are shown in Fig. 2(b). The linear transmission was normalized with respect to a reference straight plasmonic waveguide (shown in Fig. 2(a)), which is the standard method widely used to study the linear transmission properties of plasmonic nanocavities.[19] The spot size of the incident laser beam was about 4 μm, which ensures nearly equal average excitation intensity for the coupling gratings of both the plasmonic coupled-nanocavities sample and the reference waveguide. Owing to the limited tunable wavelength range of the Ti:sapphire laser system, we only measured the

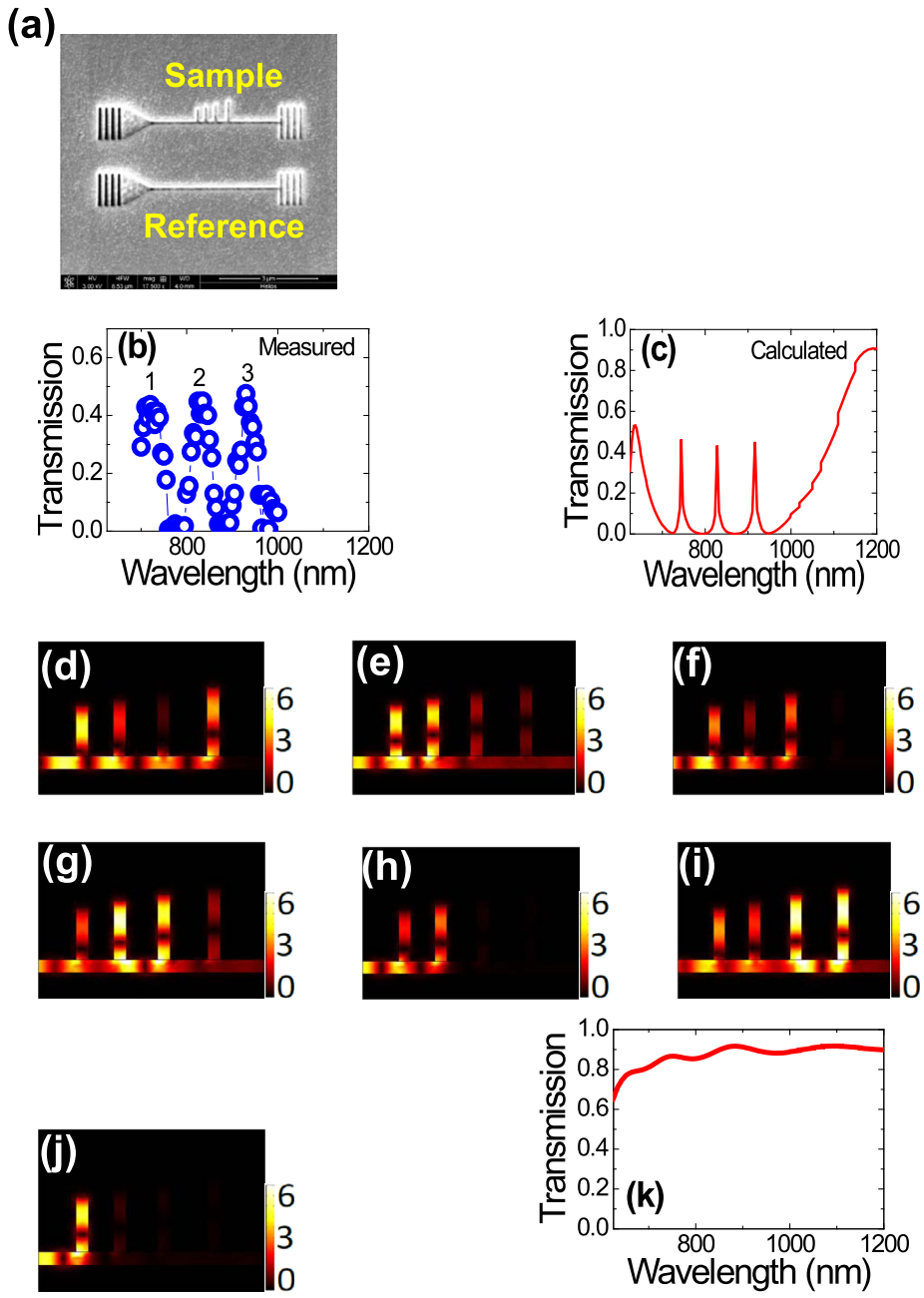

FIG. 2. (a) SEM image of the plasmonic coupled-nanocavities sample without the PMMA cover layer. Measured (b) and calculated (c) linear transmission spectrum of the plasmonic waveguide side-coupled four plasmonic coupled-nanocavities without the PMMA cover layer. Calculated magnetic field distribution of the plasmonic coupled-nanocavities without the PMMA cover layer for the incident CW light at wavelengths of 700 nm (d), 720 nm (e), 775 nm (f), 835 nm (g), 880 nm (h), 930 nm (i), and 980 nm (j). (k) Calculated linear transmission spectrum of the reference plasmonic waveguide without the PMMA cover layer.

linear transmission spectrum from 700 to 1000 nm. In the measured transmission spectrum, three sharp and high transmission peaks appeared in the transmission stop band, which indicates the formation of three transparency windows of on-chip PIT. According to the phase coupling mechanism, a transparency window can be generated when the distance between two near-neighboring nanocavities coupled via the plasmonic waveguide is equal to the integer half-wavelength of the guided SPP mode.[13] Three transparency windows will be formed when four different plasmonic nanocavities are placed in series along the plasmonic waveguide, as confirmed by the calculations of Chen *et al.*[14] The transparency windows construct perfect optical channels of the filter. The central wavelength was 720 nm for optical channel 1, 835 nm for optical channel 2, and 930 nm for optical channel 3. The line width was 46.9 nm for optical channel 1, 48.5 nm for optical channel 2, and 46.6 nm for optical channel 3, which implies that the multichannel filter possesses excellent wavelength resolution. The transmission contrast between the optical channel center and the stop band was 40%. These evidences indicate that the multichannel filter has perfect filtering properties. The measured results are in agreement with the calculated ones by using the finite element method, as shown in Fig. 2(c). The measured line width of the optical channels was more than 40 nm, which is much larger than that of the calculated one, 8 nm. The discrepancy originates from the additional losses caused by the large surface roughness of gold film and the imperfectly etched plasmonic nanocavities, as shown in Fig. 2(a). To confirm the physical mechanism of three transparency windows, we calculated the magnetic field distribution of the plasmonic coupled-nanocavities for the incident light at wavelengths of 700, 720, 775, 835, 880, 930, and 980 nm, respectively. For the incident light at wavelengths of 700,

775, 880, and 980 nm (all situated in the transmission minimum of on-chip PIT), the magnetic field distribution was mainly confined within plasmonic nanocavities, and no SPP modes could propagate through the plasmonic waveguide, as shown in Figs. 2(d), 2(f), 2(h), and 2(j), respectively. This indicates that the plasmonic resonances of nanocavities contribute to the formation of on-chip PIT. While for the incident light at wavelengths of 720, 835, and 930 nm (all situated in the transmission maximum of on-chip PIT), the magnetic field distribution was mainly confined within two near-neighboring nanocavities, and there was strong SPP mode propagating through the plasmonic waveguide, as shown in Figs. 2(e), 2(g), and 2(i), respectively. This confirms that the on-chip PIT is generated based on the phase coupling mechanism. Our calculated results was also confirmed by the calculations of Kekatpure *et al.* and Chen *et al.*[13,14] To further confirm the measured results, we calculated the linear transmission spectrum (Fig. 2(k)) of the reference plasmonic waveguide without the PMMA cover layer by using the finite element method. Nearly equal transmission of as high as 80% in the wide wavelength range from 700 to 1000 nm was obtained, as shown in Fig. 2(k).

To study the tunability of the multichannel filter, we measured the linear transmission spectrum of the plasmonic waveguide side-coupled four plasmonic nanocavities covered with a 100-nm-thick PMMA layer by using the nano-spectroscopy measurement system. In our experiment, we adopted PMMA powder with an average molecular weight of 10 000 (J&K Company, China), which was dissolved in chloroform with a weight ration of 1:100. Spin coating was used to fabricate 100-nm-thick PMMA layer on the surface of the plasmonic coupled-nanocavities sample. The measured linear transmission spectrum is depicted in Fig. 3(a). The central wavelengths of optical channels shifted in the long-wavelength direction when the plasmonic coupled-nanocavities were covered with the PMMA layer. Mulvaney has pointed out that the resonance properties of plasmonic nanostructures were enormously influenced by the refractive index of the ambient dielectric material.[24] When the PMMA layer was covered on the surface of the plasmonic coupled-nanocavities, the refractive index of the ambient dielectric material increased, which makes the plasmonic resonances provide by the nanocavities shift in the long-wavelength direction. As a result, the transparency windows also shift in the long-wavelength direction. When the PMMA layer was covered on the surface of the plasmonic coupled-nanocavities, the central wavelength of optical channel 1 changed from 720 to 765 nm, spanning a 45 nm wavelength range; that of optical channel 2 changed from 835 to 860 nm, spanning a 25 nm wavelength range; while that of optical channel 3 changed from 930 to 945 nm, spanning a 15 nm wavelength range. The differences may originate from different field distribution in the plasmonic nanocavities, as shown in Figs. 2(d)–2(j). The transmission contrast between the optical channel and the stop band was over 40%. The line width was about 45 nm for three optical channels. The measured results are in agreement with the calculated ones by using the finite element method, as shown in Fig. 3(b). This indicates that perfect filtering properties were maintained when the plasmonic coupled nanocavities were covered with the PMMA layer. These evidences confirm the excellent tunability of the multichannel filter.

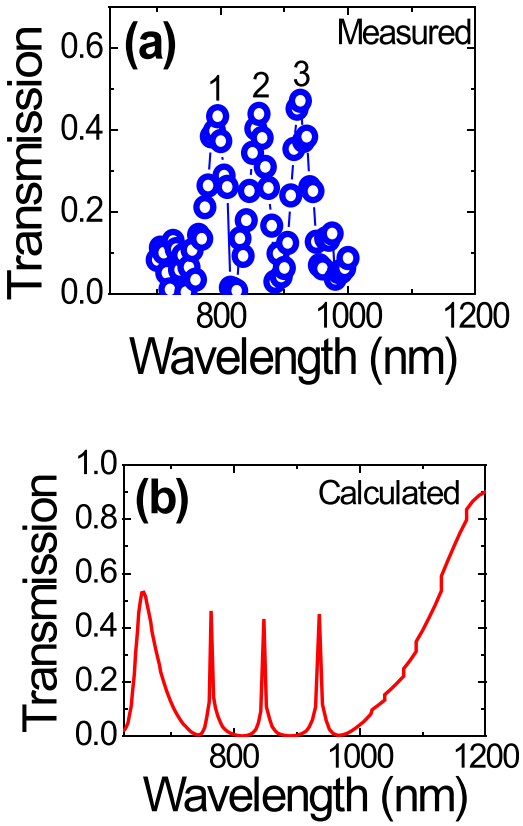

FIG. 3. Measured (b) and calculated (c) linear transmission spectrum of the plasmonic waveguide side-coupled four plasmonic coupled-nanocavities covered with a 100-nm-thick PMMA layer.

To study the thermal tunability of the multichannel filter, we calculated the linear transmission spectrum of the plasmonic waveguide side-coupled four plasmonic nanocavities covered with the 100-nm-thick PMMA layer when the ambient temperature changed by using the finite element method, and the calculated results are shown in Fig. 4. The central wavelengths of three optical channels shifted in the short-wavelength direction with the increment of the ambient temperature. Diemeer *et al.* have pointed out that PMMA has a negative value of thermo-optic coefficient dn/dT, $-1.2 \times 10^{-4}\,^{\circ}C^{-1}$.[25] Therefore, the refractive index of PMMA decreases with the increase of the ambient temperature, which makes the transparency windows shift in the

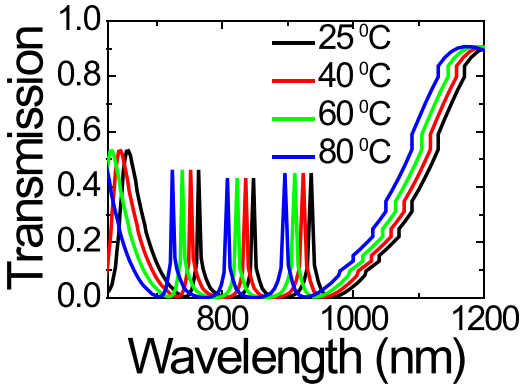

FIG. 4. Calculated transmission spectrum of the plasmonic waveguide side-coupled four plasmonic coupled-nanocavities covered with a 100-nm-thick PMMA layer at different ambient temperatures.

short-wavelength direction. When the ambient temperature increased from 25 to 80 °C, the central wavelength of optical channel 1 changed from 765 to 725 nm; that of optical channel 2 changed from 860 to 820 nm; while that of optical channel 3 changed from 945 to 905 nm. A large shift of 40 nm in the central wavelengths of optical channels can be obtained. Gosciniak *et al*. have pointed out that the response time τ of the thermo-optic effect of PMMA can be estimated by the relation[26]

$$\tau \propto \frac{\rho d h^2}{\sigma}, \tag{3}$$

where $\sigma = 0.2$ W/mK is the thermal conductivity of PMMA, $\rho = 1$ J/gK is the heat capacitance of PMMA, $d = 1$ g/cm^3 is the mass density of PMMA, and h is the thickness of PMMA layer. Owing to the relatively large thermal conductivity and small heat capacitance of PMMA, the response of the thermo-optic effect of PMMA is in several microseconds order, which has been confirmed by the measurements of Diemeer *et al*.[25] Therefore, a fast thermally tunable multichannel filter with a large tunability can be realized. Li *et al*. noted that PMMA could possess excellent and robust thermo-optic properties within the temperature range from 25 to 85 °C, which is far away from the glass transition temperature T_g of PMMA, 105 °C.[27] Diemeer also pointed that the thermo-optic properties of PMMA does not has any change even after PMMA suffering repetitive heating and cooling for up to 10×10^6 times within the temperature range from 25 to 85 °C,[28] which is confirmed by the measurements of Wang *et al*.[29] Therefore, the thermo-optic properties of PMMA do not deteriorate even after repetitive heating and cooling of the PMMA film within the temperature range from 25 to 80 °C.

In conclusion, we have experimentally realized an ultracompact chip-integrated multichannel filter in four plasmonic coupled-nanocavities. The feature device size was only 1.35 μm. A shift of 45 nm in the central wavelengths of optical channels was obtained when the plasmonic coupled-nanocavities were covered with a 100-nm-thick PMMA layer. This may be useful for the study of solid quantum chips, integrated photonic devices, and integrated photonic circuits based on plasmonic nanostructures.

This work was supported by the 973 Program of China under Grant Nos. 2013CB328704 and 2014CB921003, the National Natural Science Foundation of China under Grant Nos. 11225417, 11134001, 11121091, and 90921008, and the Program for NCET in University.

[1]A. Artar, A. A. Yanik, and H. Altug, Nano Lett. **11**, 1685 (2011).
[2]J. Zhang, W. L. Bai, L. K. Cai, Y. Xu, G. F. Song, and Q. Q. Gan, Appl. Phys. Lett. **99**, 181120 (2011).
[3]T. Utikal, T. Zentgraf, T. Paul, C. Rockstuhl, F. Lederer, M. Lippitz, and H. Giessen, Phys. Rev. Lett. **106**, 133901 (2011).
[4]T. Zentgraf, S. Zhang, R. F. Oulton, and X. Zhang, Phys. Rev. B **80**, 195415 (2009).
[5]N. Papasimakis, V. A. Fedotov, N. I. Zheludev, and S. L. Prosvirnin, Phys. Rev. Lett. **101**, 253903 (2008).
[6]P. Tassin, L. Zhang, T. Koschny, E. N. Economou, and C. M. Soukoulis, Phys. Rev. Lett. **102**, 053901 (2009).
[7]A. E. Çetin, A. Artar, M. Turkmen, A. A. Yanik, and H. Altug, Opt. Express **19**, 22607 (2011).
[8]R. Taubert, M. Hentschel, J. Kastel, and H. Giessen, Nano Lett. **12**, 1367 (2012).
[9]R. Singh, I. A. I. Alnaib, Y. P. Yang, D. R. Chowdhury, W. Cao, C. Rockstuhl, T. Ozaki, R. Morandotti, and W. Zhang, Appl. Phys. Lett. **99**, 201107 (2011).
[10]Z. Y. Li, Front. Phys. **7**, 601 (2012).
[11]Y. R. He, H. Zhou, Y. Jin, and S. L. He, Appl. Phys. Lett. **99**, 043113 (2011).
[12]J. J. Chen, Z. Li, S. Yue, J. H. Xiao, and Q. H. Gong, Nano Lett. **12**, 2494 (2012).
[13]R. D. Kekatpure, E. S. Barnard, W. Cai, and M. L. Brongersma, Phys. Rev. Lett.**104**, 243902 (2010).
[14]J. J. Chen, C. Wang, R. Zhang, and J. H. Xiao, Opt. Lett. **37**, 5133 (2012).
[15]X. Piao, S. Yu, and N. Park, Opt. Express **20**, 18994 (2012).
[16]Z. H. Han and S. I. Bozhevolnyi, Opt. Express **19**, 3251 (2011).
[17]H. Lu, X. M. Liu, D. Mao, Y. K. Gong, and G. X. Wang, Opt. Lett. **36**, 3233 (2011).
[18]A. E. Cetin, A. A. Yanik, A. Mertiri, S. Erramilli, O. E. Mustecaplioglu, and H. Altug, Appl. Phys. Lett. **101**, 121113 (2012).
[19]Z. H. Han, C. E. G. Ortiz, I. P. Radko, and S. I. Bozhevolnyi, Opt. Lett. **38**, 875 (2013).
[20]F. Zhang, X. Y. Hu, H. Yang, and Q. H. Gong, Appl. Phys. Lett. **104**, 131110 (2014).
[21]X. E. Li, T. Jiang, L. F. Shen, and X. H. Deng, Appl. Phys. Lett. **102**, 031606 (2013).
[22]P. B. Johnson and R. W. Christy, Phys. Rev. B **6**, 4370 (1972).
[23]Y. L. Fu, X. Y. Hu, C. C. Lu, S. Yue, H. Yang, and Q. H. Gong, Nano Lett. **12**, 5784 (2012).
[24]P. Mulvaney, Langmuir **12**, 788 (1996).
[25]M. B. J. Diemeer, J. J. Brons, and E. S. Trommel, J. Lightwave Technol. **7**, 449 (1989).
[26]J. Gosciniak, S. I. Bozhevolnyi, T. B. Andersen, V. S. Volkov, J. K. Hansen, L. Markey, and A. Dereux, Opt. Express **18**, 1207 (2010).
[27]X. Li, Z. Q. Cao, Q. S. Shen, and Y. F. Yang, Mater. Lett. **60**, 1238 (2006).
[28]M. B. J. Diemeer, Opt. Mater. **9**, 192 (1998).
[29]X. B. Wang, J. Sun, Y. F. Liu, J. W. Sun, C. M. Chen, X. Q. Sun, F. Wang, and D. M. Zhang, Opt. Express **22**, 11119 (2014).